Physics Letters B 797 (2019) 134808

Contents lists available at ScienceDirect

Physics Letters B

www.elsevier.com/locate/physletb

Transport model studies on the fast fission of the target-like fragments in heavy ion collisions

Qianghua Wu [a], Xinyue Diao [a], Fenhai Guan [a], Yijie Wang [a], Yingxun Zhang [b], Zhuxia Li [b], Xizhen Wu [b], Krzysztof Pomorski [c], Zhigang Xiao [a,*]

[a] Department of Physics and Collaborative Innovation Center of Quantum Matter, Tsinghua University, Beijing 100084, China
[b] China Institute of Atomic Energy, P.O. Box 275(18), Beijing 102413, China
[c] Uniwersytet Marii Curie Skłodowskiej, Katedra Fizyki Teoretycznej, 20031 Lublin, Poland

ARTICLE INFO

Article history:
Received 27 April 2019
Received in revised form 2 July 2019
Accepted 24 July 2019
Available online 26 July 2019
Editor: W. Haxton

Keywords:
Fast fission
Target like fragment
Heavy ion collisions

ABSTRACT

The fission of the target-like fragments (TLF) in heavy ion collisions (^{40}Ar+^{197}Au, b=8 fm) at beam energies from 20 to 40 MeV/u has been studied by an improved quantum molecular dynamics model (ImQMD). The time scale at a few 100 fm/c (10^{-21} s) of the TLF fission is consistent with the picture that fast fission occurs. The dynamic feature of the fast fission is illustrated by the mass asymmetry and the angular distribution of the fission axis. The effect of the surface energy coefficient and the beam energy on the dynamic feature of the fission is demonstrated. At higher beam energy, or with larger surface energy coefficient, the mass asymmetry of the fission fragments is larger and the angular distribution of the fission axis shows a more pronounced peak near beam direction, coincidentally the fission time scale is shorter. The variation suggests that the fission observables can be used as sensitive probes to the surface energy coefficient of nucleus. Irrelevant to the beam energy or the surface energy coefficient, the mean value of the relative velocity of the fission fragments situates in the vicinity of 2.4 cm/ns, in accordance with the Viola systematics applied in statistic fission. This value can be used as a calibration constant in all heavy ion fission experiments. The studies demonstrate the applicability of the transport model in the description of fast fission as a large amplitude collective motion mode in heavy ion collisions.

1. Introduction

The nuclear fission is a large-amplitude collective motion mode attracting constantly the attention of the scientists worldwide since its discovery some eighty years ago [1,2]. In nuclear physics, fission represents an ideal laboratory for probing fundamental nuclear properties and nuclear dynamics. In astrophysics, the connection of nuclear fission with the r-process is well established. It is recently believed that the abundance of the nuclide in $A \approx 160$ region is closely related to the recycling of the fission products in the r-process [3–5]. The influence of fission on the possibility to access the most exotic regions of the nuclear chart, such as the island of super-heavy elements, as well as the extreme limits in neutron richness, has turned out to be a key factor in the development of several accelerator facilities worldwide.

The fast fission phenomenon, i.e., fission without barrier, has been identified since nearly four decades [6–10]. Unlike the statistic fission, fast fission is characterized with much shorter time scale, wider fragment mass distribution and larger mass asymmetry of the fission fragments [8,11,12]. Besides the known quantum feature of the fission system such as pairing effect [13], deformation [14–16], strong dynamic feature presents with such high excitation energy or angular momentum. Very recently, isospin-dependent particle emission hierarchy has been observed in fast fission events in heavy ion collisions (HICs) at Fermi energies [17], the enhanced neutron emission from the neck region is utilized as a sensitive probe to constrain the nuclear symmetry energy at saturation density [18].

Various theoretical methods have been invented to treat the fission process with some initial excitation energy or angular momentum. The phenomenological approach of the deformation potential energy surface characterized by several shape parameters has been developed to describe the fission of both static nuclei and fast rotating deformed nuclei [19]. Recently, Fourier expansion

* Corresponding author.
E-mail address: xiaozg@tsinghua.edu.cn (Z. Xiao).

https://doi.org/10.1016/j.physletb.2019.134808

Table 1
Interaction parameters of IQ3 in ImQMD [37].

α	β	γ	C_s	g_0	g_τ	η	κ_s	ρ_0	C_0	C_1
−0.2070	0.1380	1.1667	0.0320	0.0180	0.0140	1.6666	0.080	0.1650	0.94	0.018

method has been invented to parameterize the surface shape of the extremely excited nuclei [20,21]. As the initial excitation energy and angular momentum increase, the particle emission occurs in competition with fission and hence the angular distribution of the particle with respect to the fission axis can be used to characterize the shape of the fission nuclei prior to scission point within the framework of Langevin equation [22,23]. In microscopic approaches, the spontaneous fission of ^{258}Fm has been treated in a novel stochastic mean-field framework, unraveling that the fluctuation on the total kinetic energy and the mass of the fission fragments are triggered by the quantum fluctuation, which is incorporated in the model [24]. For the nuclear reaction ^{238}U+Ca near Coulomb barrier, the complexity of the competition between the quasi fission and fusion has been investigated via time-dependent Hatree-Fock approach, particularly the influences of various ingredients including incompressibility, symmetry energy, effective nucleon mass have been analyzed by means of comparing a number of parameter sets of nuclear effective interaction [25]. Based on the energy density functional theory, the fission potential energy surface and the total kinetic energy of the fission fragments from ^{226}Th has been derived. Further, the time-dependent generalized coordinator method (TDGCM) has been developed to calculate the mass fragments distribution from the dynamic evolution of the fission system [26].

For the fission following HICs with beam energy above 10 MeV/u, where the fast fission start to contribute, microscopical transport model, which has been proved successful in describing various collective motion of HICs including fusion and flow [27–29], has been applied. The dynamic potential arising from the temporal density evolution can be described by the microscopical quantum molecular model (QMD) [30–32]. As an application, in the very heavy reaction system like ^{238}U+^{238}U, the large mass transfer and the formation of super-heavy fragments has been predicted [33–35]. Further, through the event-by-event simulations using an improved version of QMD model in the reaction ^{197}Au+^{197}Au at 15 MeV/u, various dynamic features, including the elongation of the fission necks and ternary breakup, has been demonstrated [36].

In this letter, we attempt to use the improved quantum molecular dynamics model (ImQMD) to describe the fast fission of the heavy target-like fragments (TLF) in ^{40}Ar+^{197}Au reactions at 20 to 40 MeV/u. In particular, the dynamic feature of the fast fission revealed by the mass asymmetry, the fission time scale and the relative velocity distribution are investigated. Except for the effect of the beam energy, the influence of the surface energy coefficient on various observables are emphasized.

The letter is arranged as follows. In section 2 , the framework of the ImQMD is briefly introduced. In section 3, the general dynamic feature of the fast fission process in the peripheral ^{40}Ar+^{197}Au reactions is presented. Then the influence of the beam energy and the surface energy coefficient on the fission distributions are studied. Section 4 is the summary.

2. The ImQMD model

Within the improved quantum molecular dynamics model (ImQMD), nucleons are represented by Gaussian wave packets,

$$\phi_j(\mathbf{r}) = (2\pi\sigma_r{}^2)^{-3/4} exp[-(\frac{\mathbf{r}-\mathbf{r}_j}{2\sigma_r})^2 + i\frac{\mathbf{r}\cdot\mathbf{p}_j}{\hbar}] \quad (1)$$

Here, $\mathbf{r}_j$ and $\mathbf{p}_j$ are the coordinate and momentum of the jth nucleon, σ_r is the width of wave packet in coordinate space. The nucleon evolution follows the canonical equation,

$$\mathbf{r}_j = \frac{\partial H}{\partial \mathbf{p}_j}, \mathbf{p}_j = -\frac{\partial H}{\partial \mathbf{r}_j} \quad (2)$$

where H represents the Hamiltonian containing the kinetic energy, $T = \sum_{j=1} \frac{\mathbf{p}_j{}^2}{2m}$, and the effective interaction potential energy U. The mean fields acting on these wave packets are derived from an energy density functional with the potential energy $U = U_{\rm loc} + U_{\rm Coul}$. Where $U_{\rm Coul}$ is the Coulomb energy and $U_{\rm loc} = \int H_{\rm loc}(\mathbf{r})d\mathbf{r}$ is the skyrme potential energy. The nuclear contributions $H_{\rm loc}(\mathbf{r})$ are represented in a local form with

$$H_{\rm loc} = \frac{\alpha}{2}\frac{\rho^2}{\rho_0} + \frac{\beta}{\gamma+1}\frac{\rho^{\gamma+1}}{\rho_0{}^\gamma} + \frac{g_0}{2\rho_0}(\nabla\rho)^2 + g_\tau\frac{\rho^{8/3}}{\rho_0{}^{5/3}} + \frac{C_s}{2\rho_0}[\rho^2 - \kappa_s(\nabla\rho)^2]\delta^2 \quad (3)$$

Here, $\delta = (\rho_n - \rho_p)/(\rho_n + \rho_p)$ is the isospin asymmetry, ρ_n, ρ_p are the neutron and proton densities, respectively. In the energy density functional the spin-orbit term is omitted. The interaction parameter set of IQ3 is adopted in ImQMD as listed in Table 1.

3. Results and discussions

We first analyze the time evolution of fission events and the formation of the TLFs in the peripheral ^{40}Ar+^{197}Au reactions at $b = 8$ fm. Fig. 1 presents the evolution of fast fission events in phase space. Panels (a), (b) and (c) show the evolution of one typical nuclear fast fission event at reaction time t=0, 500, 1900 fm/c in X-Z plane, respectively. Here the beam is on Z direction and X-Z plane denotes the reaction plane. At t=0 fm/c, the initial distance between the projectile and the target is 25 fm. The two colliding nuclei start to contact at about 90 fm/c followed by the rupture of the projectile-like fragments (PLF) and target like fragments before 300 fm/c. Very shortly, due to the high excitation energy and high angular momentum, the TLF undergoes the fission after some light clusters or nucleons have been emitted. As shown in Fig. 1 (b), the PLF, the two fissions fragments from the TLF and some light particles are all visible at 500 fm/c. After the scission point, while the two fission fragments fly away, light clusters and nucleons are emitted till the late stage. As in the case of t=1900 fm/c shown in Fig. 1 (c), the two fission fragments moves back to each other in central mass system.

Fig. 1 (d), (e) and (f) presents correspondingly the mass and rapidity correlation of the fission fragments in center of mass system for 10^5 simulated events. At the initial time of the reaction, t=0 fm/c, the mass number of the projectile (target) is 40 (197) and its rapidity is 1.0(−0.2) in center of mass, respectively. When the reaction proceeds to 500 fm/c, the fragments produced in the collisions are mainly distributed in two regions. In the target region, the mass range is $170 < M_f < 210$, and its rapidity is about −0.2. In the project region the mass range is $5 < M_f < 40$, and the rapidity is reduced greatly and distributes broadly near $y/y_{\rm beam} \sim 0.7$. At 1900 fm/c when most of the fast fission process are completed, as will be demonstrated from the time scale discussion, many fragments are presented in the region

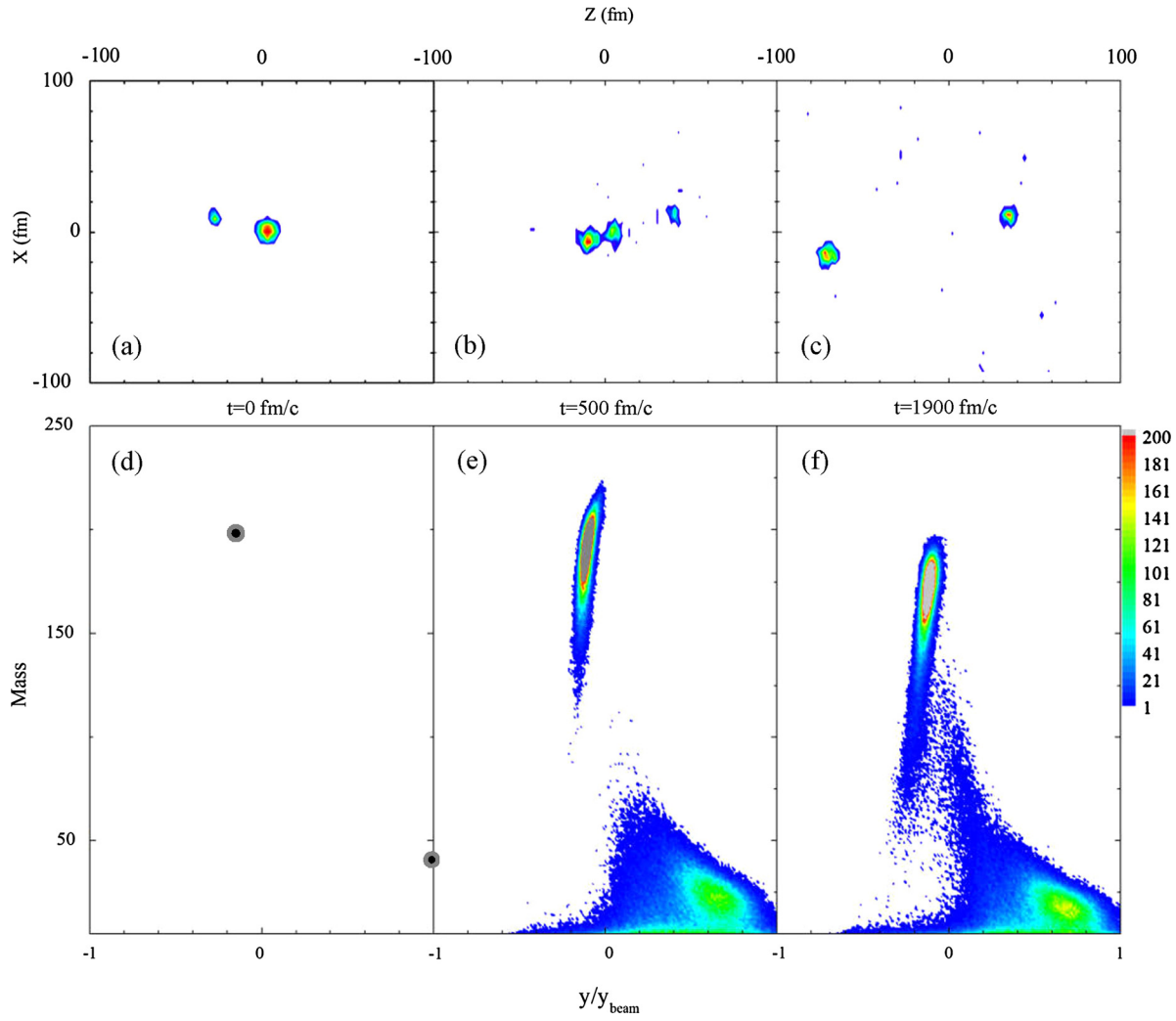

Fig. 1. A typical event and the mass-rapidity correlations in ^{40}Ar+^{197}Au at 30 MeV/u with $b = 8$ fm. Here, (a), (b) and (c) are the position distribution in coordinate space for t=0, 500 and 1900 fm/c respectively; (d), (e) and (f) are the correlation between the mass and rapidity in center of mass at the corresponding times.

of $40 < M_f < 170$ and $-0.2 < y/y_{\rm beam} < 0.2$. It is interesting to note that two components separated by a rapidity difference of $y/y_{\rm beam} \sim 0.2$ are visible in this region with the lighter fragment being emitted mainly at forward direction, indicating the dynamic feature of the fission process. Considering the above analysis and the interference of PLF, the fission fragments from TLFs must satisfy two conditions in the subsequent analysis, the mass number $M_f > 40$ and its rapidity $y/y_{\rm beam} < 0.2$.

In the heavy ion collisions at Fermi energies, incomplete fusion occurs followed by the formation of a TLF and PLF. It is interesting to survey the mass evolution of the TLF after it is produced. Fig. 2(a) presents the mass of the TLF as a function of time for the events where the TLFs do not fission. It is shown that the mass of the TLF changes from about $A \sim 180$ at initial stage to $A \sim 165$ at the late time investigated after particle emission. There are approximately 15 nucleons emitted to release the excitation energy.

During the evolution of TLF, there exists a probability for TLF to undergo fast fission. Fig. 2 (b) shows the mass asymmetry η of the two fragments from the fast fission of TLF at different time. Here η is defined as the relative mass difference of the two fragments by $\eta = (M_1 - M_2)/(M_1 + M_2)$. As one can see, for the events with fission occurring at early stage, the distribution of η peaks at large value about 0.5. As the fission time is delayed, the dynamic effect becomes less pronounced and the excitation energy of the TLF is released by particle emission, η gradually reduces. The reduction of the dynamic effect is also shown from the angular distribution of the fission axis defined by the vector of the relative velocity of the light fragment to the heavy fragment of the fast fission in center of mass system. $\theta_{\rm cm}$ shown in Fig. 2 (c) is the angle between the fission axis and the beam direction. Similarly, for the events undergoing fission early, $\theta_{\rm cm}$ mainly distributes in the range of $\theta_{\rm cm} < 90°$, indicating that the light fragments fly to forward direction while the heavy fragment fly to backward direction, keeping the memory of the incident channel. With the fission time proceeding to later stage, heavy fragments fly to forward hemisphere with an increasing probability.

Fig. 3 presents the separating time of the two fragments from the fission of TLF using different surface energy coefficients g_0 for the reactions ^{40}Ar+^{197}Au at 20 (a), 30 (b) and 40 (c) MeV/u with $b = 8$ fm. In each case 10^5 events are simulated. It is shown in all panels that the fast fission probability of TLF, represented by the differential yield y_i of the fission fragments, decreases exponentially with time. The lines are the fit using an exponential function. The results of the fission time scale τ are listed in all panels. All the values are at the order of a few hundreds fm/c (10^{-21} s). It is consistent with the fast fission time scale derived experimentally.

According to the analysis on more than 140 sets of Skyme force parameters, the surface energy coefficient is mainly distributed in

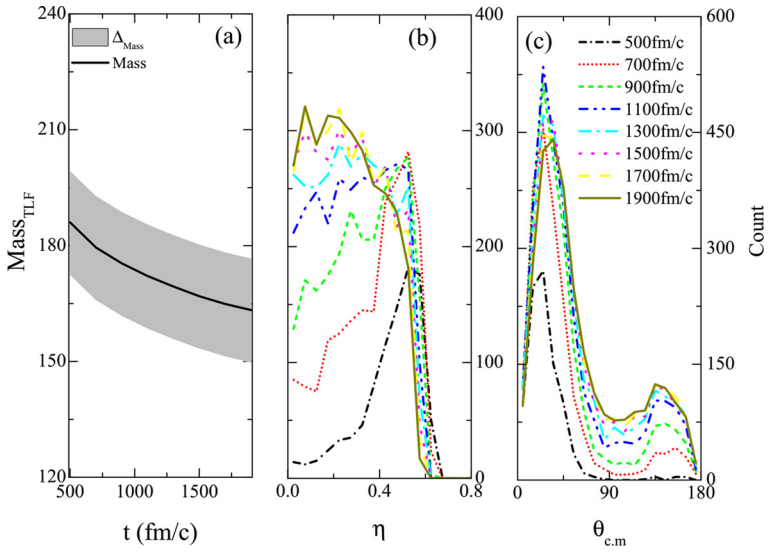

Fig. 2. (a) Mass number of TLF as a function of time, (b) the mass asymmetry distribution of fast fission fragments at different time, (c) the angular distribution of the fission axis at different time in ^{40}Ar+^{197}Au at 30 MeV/u with $b = 8$ fm.

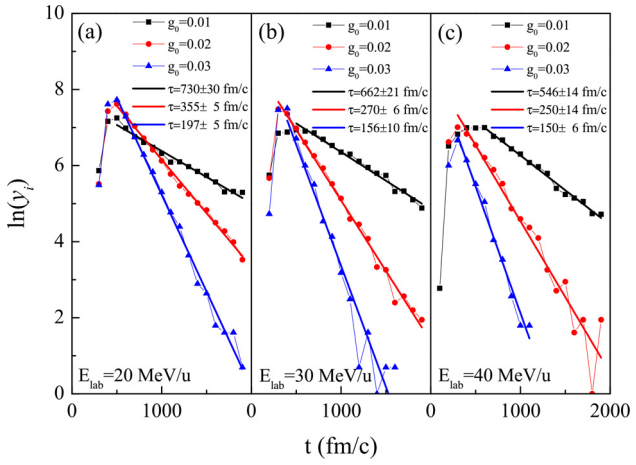

Fig. 3. The time distribution of the occurrence of fast fission in ^{40}Ar+^{197}Au at b=8 fm with $E_{\rm beam} = 20$ (a), 30 (b) and 40 (c) MeV/u, respectively. Square, dot and upper triangular symbols represent the surface energy coefficient of $g_0 = 0.01$, 0.02 and 0.03 MeV/fm^2 respectively. The black, red, and blue lines represent the exponential fit to the data points.

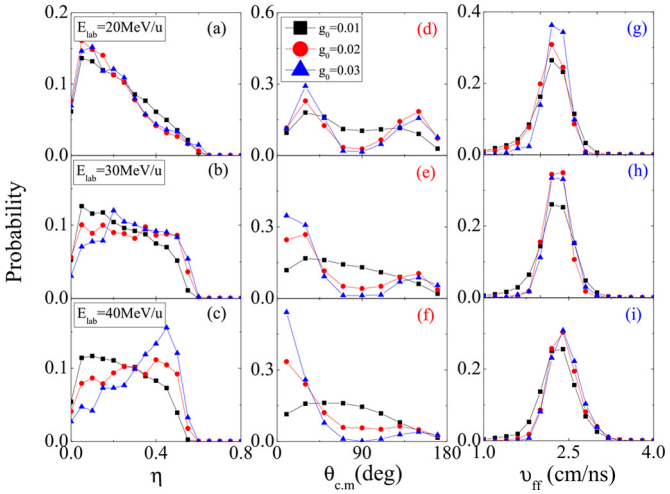

Fig. 4. Mass asymmetry η (left), fission axis angle $\theta_{\rm cm}$ (middle) and relative velocity $v_{\rm ff}$ (right) distributions of the fast fission of TLF for ^{40}Ar+^{197}Au at 20 (upper), 30 (middle) and 40 (lower) MeV/u with $b = 8$ fm, respectively. The square, circle and upper triangular symbols are corresponding to $g_0 = 0.01$, 0.02 and 0.03 MeV/fm^2 respectively.

the range from 0.01 to 0.03. So in the simulations below, three values of $g_0 = 0.01$, 0.02 and 0.03 MeV/fm^2 are used, as depicted by the different legends. Evidently, when the surface energy coefficient increases, the exponential slope becomes stiffer corresponding to shorter fission time scale. This is mainly due to the competition between Coulomb repulsion and surface tension. With a larger g_0, the surface potential energy is larger and the system favors a fast fission of TLF with larger mass asymmetry to reduce the changes of the surface area. Meanwhile the fission time scale becomes shorter.

The effect of the beam energy can be seen from the three panels (a), (b) and (c) in Fig. 3. The fission probability and the time scale τ decreases with beam energy especially for small values of the surface tension. This is mainly due to the fact that both the excitation energy and angular momentum increases with beam energy. Further, with a given g_0, the change of the time scale τ from beam energy 20 to 40 MeV/u is less obvious, compared to the effect of changing g_0 from 0.01 to 0.03 MeV/fm^2.

Further, the corresponding effect of the surface tension and the beam energy on the fission dynamics are investigated. Fig. 4 (a-c) are the mass asymmetry distribution of TLF fast fission fragments with different g_0 for ^{40}Ar+^{197}Au with b=8 fm. As one can see at 20 MeV/u, the mass asymmetry η of fission fragments is relatively small, and the influence of surface energy coefficient is insignificant. When the incident energy increase to 30 MeV/u and 40 MeV/u, the mass asymmetry increases, and the effect of the surface tension is increasingly pronounced. At 40 MeV/u with $g_0 = 0.03$ MeV/fm^2, the peak of mass asymmetry is larger than 0.4, indicating that fast fission with very large mass asymmetry is favored to suppress the change of the total surface.

Correspondingly, the angular distribution of the fission axis $\theta_{\rm cm}$ exhibits similar feature. Fig. 4 (d-f) show the distribution of $\theta_{\rm cm}$. It is clear to see from these three windows that the $\theta_{\rm cm}$ at the final time is significantly dependent on the incident energy and the surface energy coefficient. For larger surface energy coefficient $g_0 = 0.02$ and 0.03 MeV/fm^2, at 20 MeV/u, the distribution of $\theta_{\rm cm}$ shows an approximate symmetry between the forward hemisphere and the backward hemisphere. The symmetry gradually vanishes

with increasing the beam energy because dynamic effect prevails. At 40 MeV/u, most of the events situate at $\theta_{cm} < 90°$ if $g_0 \geq 0.02$, showing a strong dynamic feature. When the surface energy coefficient is $g_0 = 0.01$ MeV/fm^2, the distribution of θ_{cm} is approximately isotropic. It suggests that both the mass asymmetry, the angular distribution of the fission axis can be used as the probes to the surface energy coefficient of nucleus.

Fig. 4 (g-i) present the relative velocity v_{ff} distribution of fission fragments. It can be seen that the relative velocity of the fast fission fragments situates in 2.2-2.4 cm/ns which can be interpreted by the Viola systematics irrelevant to the surface energy coefficient nor to the beam energy. It indicates that the kinetic energies of the fission fragments are mainly contributed by the released Coulomb energy after the system passes the scission point. This quantity can be used as a robust calibration constant of the velocity difference of the fragments in fission experiment of HICs.

We note here that the raw fission observables under investigation here, including the fission probability, the fission time scale, the mass asymmetry of the fragments and the fission angular distribution, exhibit insignificant dependence on other ingredients related to the nuclear equation of state (nEOS) in the energy density functional, unlike the observations in the reactions near Coulomb barrier [25]. The reason is possibly that the fission process is much faster in the energy domain in our calculations due to the higher beam energies. It is of interest to measure the coincidental light particles which carry the information of nEOS [18,38,39].

4. Summary

To summarize, improved quantum molecular dynamics (ImQMD) model has been used to simulate the fission events in semi-peripheral ^{40}Ar+^{197}Au collision with $b = 8$ fm at Fermi energies. The distribution of the fission time exhibits an exponential distribution, with the time scale being a few hundreds fm/c in accordance with occurrence of fast fission. With increasing the beam energy leading to high excitation energy and high angular momentum, or increasing the surface energy coefficient leading to large surface tension, the dynamic feature of the fast fission becomes more pronounced. The results suggest that the mass asymmetry and the orientation of the fission axis, which can be measured experimentally, can be used as probes to study the surface energy coefficient of nucleus. It is also found that, despite of the dynamic effect of the fast fission, the distribution of the relative velocity of the two fission fragments satisfies the Viola systematics, of which the validity has been confirmed in statistical fission process. It suggests that the mean value of the relative velocity can be used as a robust calibration constant in fast fission experiments of HIC at intermediate energies. The studies extend the applicability of microscopic transport model to fast fission as a large amplitude collective motion in nuclear physics.

Acknowledgements

This work is supported by the National Natural Science Foundation of China (Grant No. 11875174 and 11890712), National Basic Research Program of China (Grant No. 2007CB209900), the Scientific Research Foundation for the Returned Overseas Chinese Scholars, Ministry of Personnel (Grant No. MOP2006138) and the Polish National Science Center (Grant No. 2018/30/Q/ST2/00185). K. Pomorski is supported by Tsinghua Global Scholar Fellowship program during his stay in Tsinghua University.

References

[1] L. Meitner, O.R. Frisch, Nature 143 (1939) 239.
[2] N. Bohr, J.A. Wheeler, Phys. Rev. 56 (1939) 426.
[3] G. Lorusso, et al., Phys. Rev. Lett. 114 (2015) 192501.
[4] N. Nishimura, et al., Phys. Rev. C 85 (2012) 048801.
[5] T. Suzuki, et al., Phys. Rev. C 85 (2012) 015802.
[6] C. Gregoire, et al., Nucl. Phys. A 387 (1982) 37.
[7] C. Gregoire, et al., Nucl. Phys. A 383 (1982) 392.
[8] P. Gläissel, et al., Z. Phys. A 310 (1983) 189.
[9] S. Leray, et al., Nucl. Phys. A 423 (1984) 175.
[10] Z. Zheng, et al., Nucl. Phys. A 422 (1984) 447.
[11] A.A. Stefanini, et al., Z. Phys. A 351 (1995) 167.
[12] F. Bocage, et al., Nucl. Phys. A 676 (2000) 391.
[13] H. Abusara, J. Phys. Conf. Ser. 869 (2017) 012051.
[14] R. Vandenbosch, K.L. Wolf, J. Unik, et al., Phys. Rev. Lett. 19 (1967) 1138.
[15] I.I. Gontchar, R.A. Kuzyakin, Phys. Rev. C 84 (2011) 014617.
[16] M. Kaur, et al., Phys. Rev. C 86 (2012) 064610.
[17] R.S. Wang, Y. Zhang, et al., Phys. Rev. C 89 (2014) 064613.
[18] Y. Zhang, J.L. Tian, et al., Phys. Rev. C 95 (2017) 041602(R).
[19] K. Pomorski, J. Bartel, Int. J. Mod. Phys. E 15 (2006) 417.
[20] K. Pomorski, et al., Acta Phys. Pol. B, Proc. Suppl. 8 (2015) 667.
[21] C. Schmitt, et al., Phys. Rev. C 95 (2017) 034612.
[22] K. Pomorski, et al., Nucl. Phys. A 605 (1996) 87.
[23] P. Schuurmans, et al., Phys. Rev. Lett. 82 (1999) 4787.
[24] Y. Tanimura, D. Lacroix, S. Ayik, Phys. Rev. Lett. 118 (2017) 152501.
[25] H. Zheng, et al., Phys. Rev. C 98 (2018) 024622.
[26] H. Tao, et al., Phys. Rev. C 96 (2017) 024319.
[27] Kai Wen, et al., Phys. Rev. Lett. 111 (012501) (2013).
[28] P. Russotto, et al., Phys. Lett. B 697 (2011) 471.
[29] C. Rizzo, et al., Phys. Rev. C 83 (2011) 014604.
[30] Junlong Tian, X. Li, et al., Eur. Phys. J. A 42 (2009) 105.
[31] Junlong Tian, Li Ou, et al., Int. J. Mod. Phys. E,20 (2011) 1755.
[32] Li Cheng, Junlong Tian, et al., Chin. Phys. C,37 (2013) 114101.
[33] Junlong Tian, Xizhen Wu, et al., Phys. Rev. C 77 (2008) 064603.
[34] Cheng Li, Junlong Tian Li Ou, et al., Phys. Rev. C 87 (2013) 064615.
[35] Ning Wang, Junlong Tian, et al., Phys. Rev. C 84 (2011) 061601(R).
[36] Junlong Tian, X.Z. Wu, Z.X. Li, et al., Phys. Rev. C 82 (2010) 054608.
[37] V. Zanganeh, N. Wang, O.N. Ghodsi, Phys. Rev. C 85 (2012) 034601.
[38] Z.Q. Feng, Phys. Rev. C 94 (2016) 014609.
[39] M. Kaur, S. Gautam, R.K. Puri, Nucl. Phys. A 955 (2016) 133.